

A Transition Edge Sensor Operated in Coincidence with a High Sensitivity Phonon Veto for Photon Coupled Rare Event Searches

R.K. Romani,^{1, a)} Y.-Y. Chang,¹ R. Mahapatra,² M. Platt,² M. Reed,¹ I. Rydstrom,¹ B. Sadoulet,¹ B. Serfass,¹ and M. Pyle¹

¹⁾University of California Berkeley, Department of Physics, Berkeley, CA 94720, USA

²⁾Texas A&M University, Department of Physics and Astronomy, College Station, TX 77843-4242, USA

(*Electronic mail: rkromani@berkeley.edu.)

(Dated: 08/20/24)

Experimental searches for axions or dark photons that couple to the standard model photon require photosensors with low noise, broadband sensitivity, and near zero backgrounds. Here, we introduce a Transition Edge Sensor (TES) based photon sensor with a high sensitivity athermal phonon sensor coupled to the substrate on which the TES is deposited. We show that single photons absorbed locally in the TES have $\sim 35\%$ energy deposition in the electronic system of the TES, with $\sim 26\%$ of the photon energy absorbed by the athermal phonon sensor (due to athermal phonons leaking out of the TES during the downconversion process). Backgrounds are observed to be largely coupled to either the TES or phonon system. At high energies, these backgrounds can be efficiently discriminated from TES photon absorption events, while at low energies, their leakage into the passage band is well modeled. With significant sensitivity improvements to both the photon and phonon channel, this coincidence technique could be used to suppress backgrounds in bosonic dark matter searches down to energies near the superconducting bandgap of the sensor.

Multiple tests of Beyond the Standard Model (BSM) physics search for the coupling of proposed BSM particles to a standard model (SM) photon. In “dish antenna” type searches for axion dark matter¹ (e.g. BRASS², BREAD³), high magnetic fields coupled to reflectors attempt to convert dark matter halo axions or axion-like-particles to SM photons via the inverse-Primakoff effect. In contrast, “light shining through walls” type experiments (e.g. ALPS⁴) convert SM photons to axions or axion-like-particles through the Primakoff process before converting them back into SM photons through the inverse-Primakoff effect. Finally, other experimental architectures search for photon conversion in dielectric stacks (e.g. LAMPPOST⁵, MADMAX⁶).

In all three experimental architectures, tests of BSM physics rely on the the ability to search for rare photons using high performance photon sensors. Such sensors would ideally have large dynamic range (to test the maximum possible particle mass/energy range), low noise (to search for the smallest energy photons), and have near zero background rate that is indistinguishable from the BSM signal.

Transition Edge Sensors (TESs)⁷ are a mature, low noise, relatively large dynamic range sensor technology which have been proposed for use in such photon coupled rare event searches^{3,8} and demonstrated as astronomical sensors^{9,10}. However, recent high-performance TES based dark matter calorimeters have measured a background rate of events¹¹ which seem to originate in the sensor^{12,13}. In photon coupled rare event searches, these events would mimic those expected from e.g. axions converting to SM photons, constituting a limiting background. In this letter, we propose and demonstrate a sensor architecture designed to measure both the localized energy deposited in the TES electronic system

and the phonon energy dropped into the substrate by a photon absorbed by the TES. Requiring coincidence of these two signals discriminates real TES photon absorption from both non-ionizing phonon backgrounds and backgrounds which entirely deposit their energy in the sensor electronic system.

Photon interactions with TESs are commonly modeled by assuming that the photon initially transfers all its energy to a single electron, which quickly downconverts to a large number of excited electrons (i.e. quasiparticles) and phonons.¹⁴ This electron-phonon cascade process ultimately results in an elevated thermal energy in the TES electronic system that is responsible for the TES response. During this downconversion process, energy is lost when phonons radiated from excited electrons have low enough energy to escape the TES into the substrate. Previous estimates¹⁵ have indicated that the photon energy is roughly equally partitioned between the TES electronic system and the phonons lost to the substrate, broadly consistent with previous measurements of the fraction of optical photon energy absorbed locally in TESs⁹. However, the fraction of radiated phonons that can break aluminum Cooper pairs and thus be sensed by superconducting athermal phonon detectors has never been measured.

Here, we introduce a $200 \mu\text{m} \times 800 \mu\text{m} \times \sim 40 \text{ nm}$ $65.1 \pm 0.2 \text{ mK}$ effective T_c W TES with a $\sigma_{\text{TES}} = 128.5 \pm 0.1 \text{ meV}$ energy resolution for Dirac-delta energy depositions within the TES, patterned on a $1 \text{ cm} \times 1 \text{ cm} \times 1 \text{ mm}$ thick silicon substrate instrumented with an athermal phonon sensor (see Fig. 1). The athermal phonon veto sensor is constructed by coupling an array of W TESs to aluminium athermal phonon collection fins in the common QET architecture¹⁶. Approximately 64.3% percent of the phonon-absorbing metal on the detector surface is composed of active athermal phonon sensors, while the TES used to absorb optical photons makes up only $\sim 1.07\%$ percent of the metal on the device surface. Because of this difference in coverage fraction, photon events absorbed in the substrate will predominantly couple to the

^{a)}Corresponding author: rkromani@berkeley.edu

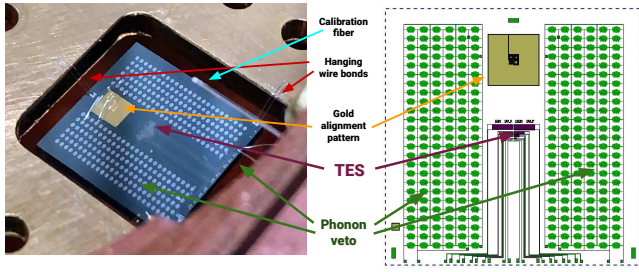


FIG. 1. (Left) Photograph of our TES with thermal phonon veto chip mounted in the cryostat. Note that the device is suspended from wire bonds (see text), and illuminated from above by a fiber with a diffusing tip. (Right) The design of the device. Note that only the top right (i.e. $200\ \mu\text{m}$ by $800\ \mu\text{m}$) TES is read out for this study.

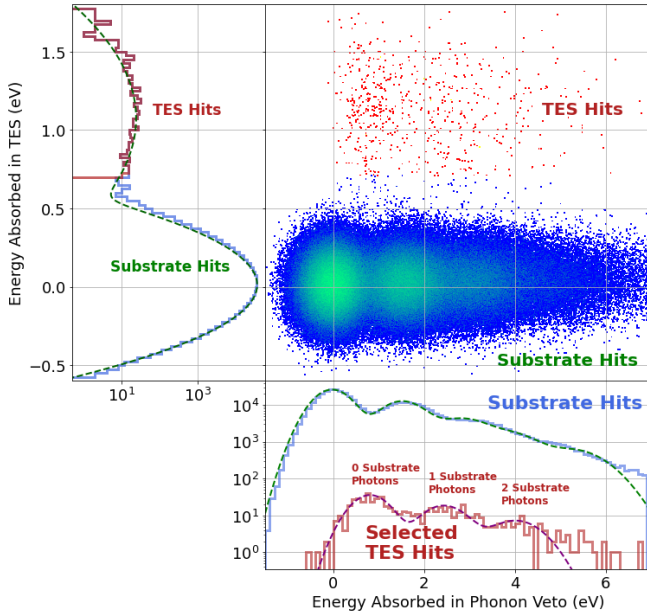


FIG. 2. (Main) Heatmap plot of the energies absorbed in the TES and phonon veto from $3.061\ \text{eV}$ photon calibration events, each point corresponds to the device response from one photon calibration pulse. Most photons hitting the device are absorbed in the substrate phonon system, leading to large response in the phonon veto with essentially no response in the TES (blue/green points). Rarely, photons directly hit the TES, creating a large response (red points). (Left) Histogram of energies absorbed in the TES. (Bottom) Histogram of energies in the phonon veto for all events (blue) and events which are tagged as TES hits (red). Dashed lines show Gaussian fits.

phonon readout; very little response is expected in the TES. Our device is suspended by wire bonds as in Ref.¹⁷ in order to suppress “Low Energy Excess” (LEE) backgrounds associated with gluing the substrate to a copper mount.

To calibrate the device response, we illuminate the entire device surface with pulses of $405\ \text{nm}$ ($3.061\ \text{eV}$) photons with an average of $\lambda = 0.165 \pm 0.012$ photons per bunch. We trigger on a TTL signal which is coincident with the laser pulse, and measure the response in our TES and phonon veto channels using an optimal/matched filtering approach (see Fig. 2).

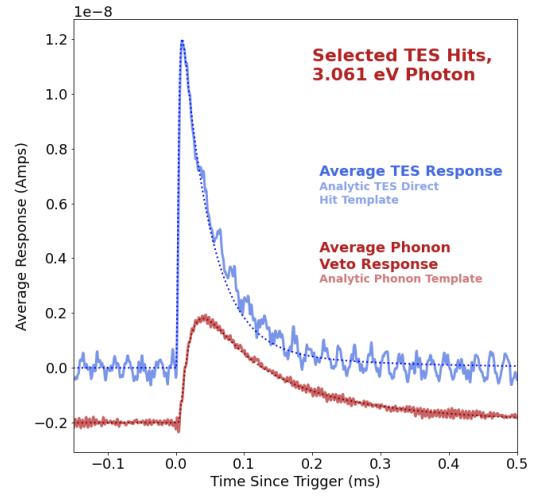


FIG. 3. The average time domain response in the TES (blue) and phonon veto (red) channels for events where a single photon is absorbed in the TES and no photon is absorbed in the detector phonon system (events labeled “0 Substrate Photons” in Fig. 2). Note the nonzero response in the phonon veto channel. For clarity, averaged responses are low pass filtered ($f_{\text{cut}} = 100\ \text{kHz}$), and responses are baseline-subtracted and offset. For comparison, dotted lines show modeled responses for Dirac-delta energy impulses in the TES (blue, dotted) and phonon system events in the phonon veto (red, dotted).

Most calibration photons are absorbed in the substrate phonon system, and are used to calibrate the response of the phonon veto. In the veto, we measure a phonon energy resolution of $\sigma_{\text{phonon}} = 701 \pm 2\ \text{meV}$ and a phonon collection efficiency of $\epsilon_{\text{phonon}} = 0.499 \pm 0.001$ for substrate absorbed photons.

In rare cases, a calibration photon directly hits the TES, producing a large response. Alongside this direct TES interaction, additional photons from the calibration pulse can interact with the substrate phonon system. These “TES direct hit” events can be used to study the response of the TES to optical photons and to gain insight into the downconversion process occurring in the TES.

After selecting events with a large response in the TES, we plot a histogram of coincident energies seen in the phonon veto. We fit this histogram with multiple Gaussians, corresponding to events with zero, one, two, etc. photons being absorbed in the substrate phonon system (in addition to the photon being absorbed in the TES). Notably, the zeroth peak is *not* consistent with zero response in the phonon sensor. Selecting events from this zeroth peak, and comparing their average pulse shape to templates (see Fig. 3), we see that the response in the TES channel is consistent with the modeled device response from a Dirac-delta-like energy deposition in the TES, consistent with a downconversion process which is fast compared to the $O(10\ \mu\text{s})$ TES response time. In contrast, the response in the phonon readout is consistent with the slow absorption of athermal phonons (i.e. identical to substrate events). We interpret these phonons as originating from the leakage of athermal phonons from the TES during the electronic downconversion process following the absorption of a

photon.

By fitting events in this peak (one photon absorbed in the TES, zero photons absorbed in the substrate), we measure the average partitioning of energy in the downconversion process. The energy absorbed in our TES and phonon veto for each event can be calculated by multiplying the fit optimum filter amplitude I_{OF} in units of current through the TES by a conversion factor $\frac{\partial E}{\partial I}$. This conversion factor was calculated using the normalized current domain event template $T_i(t)$ and the responsiveness of the TES $\frac{\partial P}{\partial I}(f)$, by using Fourier and inverse Fourier transforms \mathcal{F} and \mathcal{F}^{-1} to calculate the power domain template $T_p(t)$:

$$\frac{\partial E}{\partial I} = \int T_p(t) dt = \int \mathcal{F}^{-1} \left(\frac{\partial P}{\partial I}(f) \mathcal{F}(T_i(t)) \right) dt \quad (1)$$

Using this procedure, we measure the energy absorbed in both the TES and phonon veto, and find that for a 3.061 eV calibration photon direct hit on the TES, on average $f_T = 35.1 \pm 0.6 \%$ is absorbed in the TES, while $f_V = 26.4 \pm 0.8 \%$ is absorbed in the phonon veto. After accounting for photon collection efficiency, we infer a baseline resolution of $\sigma_\gamma = 368.4 \pm 0.4$ meV for photons incident on the TES. By contrast, selecting events consistent with photon absorption in the substrate only we find that $49.9 \pm 0.1 \%$ of the photon energy is collected in athermal phonon sensor and $\lesssim 1 \%$ is absorbed in the TES.

If we assume the phonon collection efficiency factor measured for substrate absorbed photons also applies to the phonons escaping the TES after a direct photon hit, we infer that $52.8 \pm 1.6 \%$ of the initial photon energy is put into the substrate phonon system as phonons with energy above the superconducting aluminum bandgap. However, the phonon spectrum created by the downconversion of phonons absorbed in the substrate phonon system is almost certainly somewhat different from the spectrum from events absorbed in the TES; therefore this number is only qualitative.

Additionally, we collected 24 hours of background data in the device, triggering on the time domain optimal filtered trace in both the TES and phonon veto channels (see Fig. 4). In this background dataset, we observed two main background types: phonon coupled backgrounds triggered in the phonon veto channel, and “singles” triggered in the TES. These observations broadly agree with previous background measurements in similar detectors of “Low Energy Excess” (LEE) type backgrounds.^{12,13}

For events triggered in the phonon veto, we observe a rising background below $\lesssim 500$ eV which we attribute to phonon coupled LEE events, while at higher energies we see saturated events which we attribute to muon- and radioactive-decay-induced high energy backgrounds. From the coupling of these “shared” or phonon coupled LEE background events to the TES and phonon veto, we can estimate that the TES collects approximately 1% of the phonon energy collected by the phonon veto. We observed that in a given energy bin, the rate of low energy backgrounds relaxes away with time, again consistent with LEE observations.

In the TES, we observe a spectrum that is consistent with random Gaussian noise below ~ 0.75 eV. Above this energy,

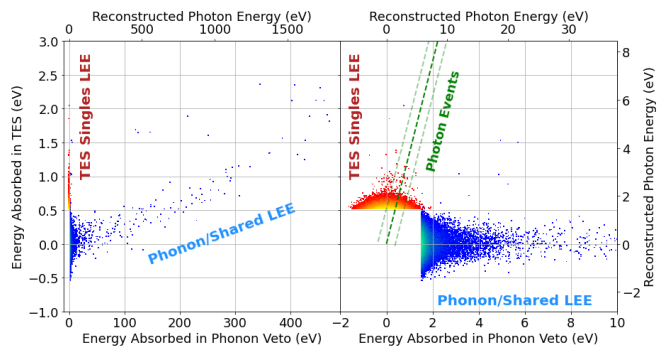


FIG. 4. The backgrounds observed in the device, triggered either on a signal in the TES (red) or in the phonon veto (blue/green). Backgrounds triggered in the phonon veto are consistent with phonon coupled Low Energy Excess (LEE). Backgrounds triggered in the TES, which we interpret as LEE “singles” seen in other devices, are consistent with a TES response from an impulse like energy deposition in the TES with little or no phonon response. (Right) is a cropped view of (left). The response consistent with photon absorption in the TES (dark green, dashed) with $\chi^2 = 1$ bands (light green, dashed, see text) is shown.

we observe a non-Gaussian outlier tail which has a pulse shape consistent with Dirac-delta impulses of energy deposited in the TES that we associate with LEE “singles.”^{12,13}

The majority of these events are inconsistent with a photon-absorption-like energy partitioning between the TES and phonon veto, leading us to discard photon backgrounds (see e.g. Ref.¹⁸) as the primary cause of LEE singles seen in our devices. Additionally, the lack of a phonon component for the majority of events indicates that any process in the TES that results in a phonon or electron downconversion cascade from energies much greater than the superconducting bandgap is not a viable explanation for the majority of singles LEE events. A likely explanation for these events is bursts of sub aluminium bandgap photons that couple to the TES via its antenna-like bias lines. In the future, we plan to aggressively filter the TES bias lines throughout the MHz-100GHz range such that such hypothetical external EMI bursts are significantly attenuated.

Despite the presence of two unmodeled backgrounds (shared and singles LEE^{12,13}), these backgrounds can be largely cut by requiring a coincident response in the TES and phonon channels consistent with a photon being absorbed by the TES (see Fig. 5). Using inverse variance weighting, we reconstructed a photon energy

$$E_\gamma = \frac{1}{\sigma_{\gamma T}^{-2} + \sigma_{\gamma V}^{-2}} \left(\frac{E_{\gamma T}}{\sigma_{\gamma T}^2} + \frac{E_{\gamma V}}{\sigma_{\gamma V}^2} \right) \quad (2)$$

$$= \frac{1}{\sigma_T^{-2} f_T^2 + \sigma_V^{-2} f_V^2} \left(\frac{E_T / f_T}{\sigma_T^2 / f_T^2} + \frac{E_V / f_V}{\sigma_V^2 / f_V^2} \right) \quad (3)$$

where E_T (σ_T) and E_V (σ_V) are the energies absorbed (resolutions) in the TES and phonon veto respectively, and f_T and f_V are the TES and phonon veto collection efficiencies for photons absorbed in the TES (see above). We also define a

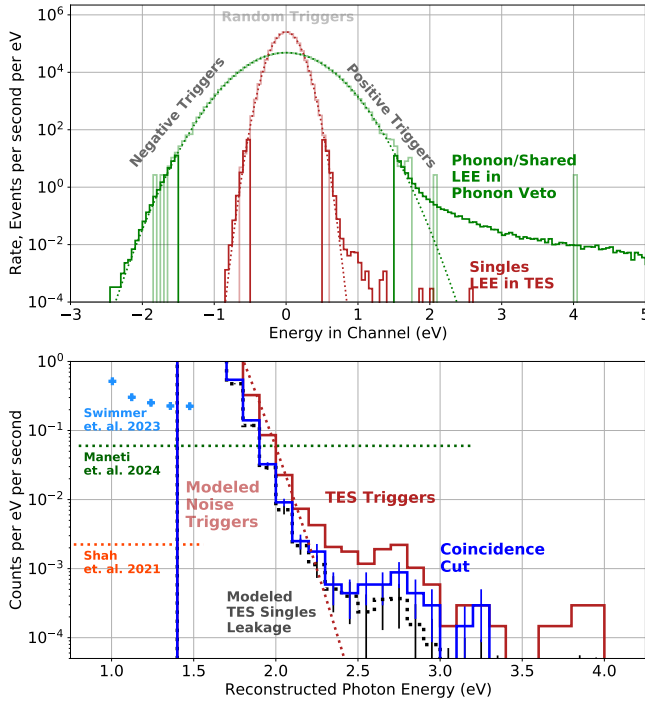


FIG. 5. (Top) Spectrum of background events observed in either the phonon veto (green) or TES (red). Solid spectra show triggers on positive or negative (noise sampling) amplitude events of significance $\geq 4\sigma$. Solid lighter color spectra show the reweighted event amplitudes of randomly triggered events, sampling the noise. Dotted lines show Gaussian fits to the negative triggers, demonstrating that random fluctuations around zero describe the observed rate of events below ~ 1.7 eV in the phonon veto and ~ 0.8 eV in the TES channel. (Bottom) Spectrum of photon-equivalent energies constructed through a weighted sum of energies in the TES and veto channels (see text) before (red) and after (dark blue) a coincidence cut requiring a response in both channels within $\chi^2_\gamma = 1$ of a photon-like response (see text). We model leakage of TES LEE singles into the acceptance band by assuming Gaussian smearing (blue dotted histogram, see text), and find that this leakage largely explains the observed number of events passing our cuts. The red dotted line shows expected rate of noise triggers. Blue, green and orange dots show the background rates measured in Refs.^{19–21}, rescaled by sensor area.^{22,23}

goodness-of-fit value for photon events

$$\chi^2_\gamma = \frac{(E_{\gamma T} - E_{\gamma V})^2}{\sigma_{\gamma T}^2 + \sigma_{\gamma V}^2} \quad (4)$$

Using this statistic, we can define a coincidence cut ($\chi^2_\gamma < 1$) designed to preferentially cut events not consistent with a photon-like energy depositions. Through Gaussian smearing in the phonon veto channel, a subset of triggers on LEE single events in the TES may appear to have phonon veto responses consistent with photon absorption in the TES. Assuming that all TES singles have phonon veto responses drawn from a Gaussian centered at zero, we model this leakage (dotted line, Fig. 5) and show that in each bin, the observed photon-like

events are consistent with Gaussian leakage of TES singles. Considering all bins, there appears to be a systematic bias towards observing more events than expected from LEE singles leakage, possibly suggesting a subdominant component of the observed background comes from true photon absorption events in the TES. Such an additional subset of events might be caused by scintillation of e.g. PCBs used to read out the device¹⁸ or by stress relaxation in the TES itself^{17,24}.

In Fig. 5 we compare our device to benchmark TES^{20,21} and MKID¹⁹ photon detectors with reported background rates. We have scaled the rates by the area of the sensor^{22,23}, as many of the hypothetical sources dark counts (stray environmental photons from insulators in the optical cavity, internal stress relaxation) would scale with the sensor area. In fact, we used a large $200\mu\text{m} \times 800\mu\text{m}$ TES (~ 3 orders of magnitude larger than a standard optical TES) to enhance these volume scaled dark count rates. At high energies, our device compares favorably or comparably to Refs.^{19–21} (assuming the backgrounds in Ref.^{19,21} remain flat to higher energies). At lower energies, the large size of our TES creates additional thermal fluctuation noise which unfortunately limits our threshold. As discussed below, simply reducing the size and T_c of our TES (as our group has already demonstrated²⁵) would be expected to significantly reduce both threshold and background level.

In this letter, we propose and demonstrate a new optical photon sensor architecture which reduces the impact of sensor-specific backgrounds by requiring that signals in a photon sensing TES be coincident with a pulse of athermal phonons created in the downconversion process in the TES. Our observation of this process supports longstanding models describing electronic thermalization in superconducting and metal films. Our architecture is ideal for photon coupled rare event searches, which search for rare photons created by BSM processes.

Future versions of this device architecture should be designed to optimize two performance metrics: the resolution and the leakage of TES singles into the passage band. Our group has already demonstrated TESs with an order of magnitude better resolution solely through decreasing our TES volume and T_c ²⁵, and no fundamental limitations prevent the operation of world leading TESs¹⁰ in devices of this type. Indeed, simply scaling our TES to $(25\mu\text{m})^2$ and 40 mK would be expected to reduce σ_γ to a world leading ~ 11 meV, essentially eliminating the random noise that limits the performance of this specific device in the mid and near IR range. More efficient vetoing of TES singles requires improving the phonon veto energy resolution, in order to tag the relatively small phonon signal originating from photons being absorbed in the photon sensing TES. Our group has already demonstrated athermal phonon detectors with twice the performance of the phonon veto in this paper, by decreasing the quantity of instrumented and non-instrumented metal coverage on the substrate surface. Furthermore, the noise of this device is completely dominated by LEE shot noise¹³, putting enormous sensitivity improvements within reach. However, we fully expect that ultimately other superconducting photon and phonon sensor technologies (e.g. KIDs²⁶, SQUATS²⁷) are likely needed to realize this coincidence tagging architecture in the far-IR.

Finally, our results shed light on the nature of LEE singles and shared events. The majority of TES only, single events must not primarily originate from a small number of high energy electrons or photons in the TES, as we do not see a coincident phonon pulse that leaks from the TES during the downconversion process; GHz scale photon bursts transmitted to the TES through the TES bias lines are a reasonable hypothesis that matches this observation. Less can be gleaned on the source of the LEE phonon bursts. If the source of the phonon LEE events was stress relaxation in the W films, we would expect a small population of events with both a TES signal (from local energy absorption in the TES electronic system) and a phonon sensor energy deposition (from dropped athermal phonons). Given the absence of such a population, if stress relaxation in the bare W film is the dominant source of phonon LEE events, the relaxation process must deposit a very small fraction of energy in the film electronic system.

ACKNOWLEDGEMENTS

This work was supported in part by DOE Grant DE-SC0019319, DE-SC0022354, and DOE Quantum Information Science Enabled Discovery (QuantISED) for High Energy Physics (KA2401032). Work at Lawrence Berkeley National Laboratory was supported by the U.S. DOE, Office of High Energy Physics, under Contract No. DEAC02-05CH11231.

REFERENCES

- ¹D. Horns, J. Jaeckel, A. Lindner, A. Lobanov, J. Redondo, and A. Ringwald, “Searching for wispy cold dark matter with a dish antenna,” *Journal of Cosmology and Astroparticle Physics* **2013**, 016–016 (2013).
- ²F. Bajjali, S. Dornbusch, M. Ekmedžić, D. Horns, C. Kasemann, A. Lobanov, A. Mkrtchyan, L. H. Nguyen, M. Tluczykont, G. Tuccari, J. Ulrichs, G. Wieching, and A. Zensus, “First results from brass-p broadband searches for hidden photon dark matter,” *Journal of Cosmology and Astroparticle Physics* **2023**, 077 (2023).
- ³J. Liu, K. Dona, G. Hoshino, S. Knirck, N. Kurinsky, M. Malaker, D. W. Miller, A. Sonnenschein, M. H. Awida, P. S. Barry, K. K. Berggren, D. Bowring, G. Carosi, C. Chang, A. Chou, R. Khatiwada, S. Lewis, J. Li, S. W. Nam, O. Noroozian, and T. X. Zhou, “Broadband solenoidal haloscope for terahertz axion detection,” *Physical Review Letters* **128** (2022), 10.1103/physrevlett.128.131801.
- ⁴K. Ehret, M. Frede, S. Ghazaryan, M. Hildebrandt, E.-A. Knabbe, D. Kracht, A. Lindner, J. List, T. Meier, N. Meyer, D. Notz, J. Redondo, A. Ringwald, G. Wiedemann, and B. Willke, “New alps results on hidden-sector lightweights,” *Physics Letters B* **689**, 149–155 (2010).
- ⁵J. Chiles, I. Charaev, R. Lasenby, M. Baryakhtar, J. Huang, A. Roshko, G. Burton, M. Colangelo, K. Van Tilburg, A. Arvanitaki, S. W. Nam, and K. K. Berggren, “New constraints on dark photon dark matter with superconducting nanowire detectors in an optical haloscope,” *Physical Review Letters* **128** (2022), 10.1103/physrevlett.128.231802.
- ⁶B. Majorovits, “Madmax: A new road to axion dark matter detection,” (2017).
- ⁷K. Irwin and G. Hilton, “Transition-Edge Sensors,” in *Cryogenic Particle Detection*, Topics in Applied Physics, edited by C. Enss (Springer, Berlin, Heidelberg, 2005) pp. 63–150.
- ⁸K.-S. Isleif, “The any light particle search experiment at desy,” *Moscow University Physics Bulletin* **77**, 120–125 (2022).
- ⁹B. Cabrera, R. M. Clarke, P. Colling, A. J. Miller, S. Nam, and R. W. Romani, “Detection of single infrared, optical, and ultraviolet photons using superconducting transition edge sensors,” *Applied Physics Letters* **73**, 735–737 (1998).
- ¹⁰K. Hattori, T. Konno, Y. Miura, S. Takasu, and D. Fukuda, “An optical transition-edge sensor with high energy resolution,” *Superconductor Science and Technology* **35**, 095002 (2022).
- ¹¹P. Adari *et al.*, “EXCESS workshop: Descriptions of rising low-energy spectra,” *SciPost Physics Proceedings*, 001 (2022).
- ¹²G. Angloher, S. Banik, G. Benato, A. Bento, A. Bertolini, R. Breier, C. Bucci, J. Burkhart, L. Canonica, A. D’Addabbo, *et al.*, “Doublets detectors to investigate the cressst low energy background: results from above-ground prototypes,” arXiv preprint arXiv:2404.02607 (2024).
- ¹³SPICE/HeRALD / TESSERACT collaboration, “Low energy backgrounds and excess noise in a two-channel low-threshold calorimeter,” (2024), in preparation.
- ¹⁴A. G. Kozorezov *et al.*, “Quasiparticle-phonon downconversion in nonequilibrium superconductors,” *Phys. Rev. B* **61**, 11807–11819 (2000).
- ¹⁵B. Cabrera and R. Romani, “Optical/UV astrophysics applications of cryogenic detectors,” in *Topics in Applied Physics* (Springer Berlin Heidelberg, 2005) pp. 417–452.
- ¹⁶K. D. Irwin, S. W. Nam, B. Cabrera, B. Chugg, and B. A. Young, “A quasiparticle-trap-assisted transition-edge sensor for phonon-mediated particle detection,” *Review of Scientific Instruments* **66**, 5322–5326 (1995).
- ¹⁷R. Anthony-Petersen *et al.*, “A Stress Induced Source of Phonon Bursts and Quasiparticle Poisoning,” (2022), arxiv:2208.02790 [cond-mat, physics:physics].
- ¹⁸P. Du, D. Egana-Ugrinovic, R. Essig, and M. Sholapurkar, “Sources of low-energy events in low-threshold dark-matter and neutrino detectors,” *Phys. Rev. X* **12**, 011009 (2022).
- ¹⁹N. Swimmer, W. H. Clay, N. Zobrist, and B. A. Mazin, “Characterizing the dark count rate of a large-format mkid array,” *Optics Express* **31**, 10775 (2023).
- ²⁰L. Manenti, C. Pepe, I. Sarnoff, T. Ibrayev, P. Oikonomou, A. Knyazev, E. Monticone, H. Garrone, F. Alder, O. Fawwaz, A. J. Millar, K. D. Morà, H. Shams, F. Arneodo, and M. Rajteri, “Study of dark counts in optical superconducting transition-edge sensors,” (2024).
- ²¹R. Shah, K.-S. Isleif, F. Januschek, A. Lindner, and M. Schott, “Tes detector for alps ii,” (2021).
- ²²P. Szypryt, S. R. Meeker, G. Coiffard, N. Fruitwala, B. Bumble, G. Ulbricht, A. B. Walter, M. Daal, C. Bockstiegel, G. Collura, N. Zobrist, I. Lipartito, and B. A. Mazin, “Large-format platinum silicide microwave kinetic inductance detectors for optical to near-ir astronomy,” *Optics Express* **25**, 25894 (2017).
- ²³J. A. Rubiera Gimeno, K.-S. Isleif, F. Januschek, A. Lindner, M. Meyer, G. Othman, M. Schott, R. Shah, and L. Sohl, “The tes detector of the alps ii experiment,” *Nuclear Instruments and Methods in Physics Research Section A: Accelerators, Spectrometers, Detectors and Associated Equipment* **1046**, 167588 (2023).
- ²⁴R. K. Romani, “Aluminium relaxation as the source of excess low energy events in low threshold calorimeters,” (2024).
- ²⁵C. W. Fink, S. L. Watkins, *et al.*, “Characterizing TES power noise for future single optical-phonon and infrared-photon detectors,” *AIP Advances* **10** (2020), 10.1063/5.0011130.
- ²⁶O. Wen, T. Aralis, R. Basu Thakur, B. Bumble, Y.-Y. Chang, K. Ramanathan, and S. R. Golwala, “Performance of a phonon-mediated detector using kids optimized for sub-gev dark matter,” *Journal of Low Temperature Physics* **209**, 510–517 (2022).
- ²⁷C. W. Fink, C. P. Salemi, B. A. Young, D. I. Schuster, and N. A. Kurinsky, “The superconducting quasiparticle-amplifying transmon: A qubit-based sensor for mev scale phonons and single thz photons,” (2023).